Erschienen in: Optics Express ; 24 (2016), 26. - S. 22930-22940
http://dx.doi.org/10.1364/OE.24.029930

Research Article | Vol. 24, No. 26 | 26 Dec 2016 | OPTICS EXPRESS 29930

Optics EXPRESS

Ultrafast time-domain spectroscopy system using 10 GHz asynchronous optical sampling with 100 kHz scan rate

OLIVER KLIEBISCH,[1,*] DIRK C. HEINECKE,[1] AND THOMAS DEKORSY[1,2]

[1]*Center for Applied Photonics, University of Konstanz, 78457 Konstanz, Germany*
[2]*Institute for Technical Physics, German Aerospace Center, Pfaffenwaldring 38-40, 70569 Stuttgart, Germany*
[*]*oliver.kliebisch@uni-konstanz.de*

Abstract: An ultrafast time-domain spectroscopy system employing asynchronous optical sampling at a repetition rate of 10 GHz is presented. Two ultra-compact Ti:sapphire femtosecond ring lasers allow to achieve scan rates as high as 100 kHz for a 100 ps long time window and a time-delay resolution of 100 fs. The feasibility of this high-speed ASOPS system is evaluated by performing THz time domain spectroscopy on molecular gases where signal-to-noise ratios exceeding 30 dB for averaging times in the millisecond range have been obtained. In order to demonstrate the benefits of this system for ultrafast pump-probe spectroscopy we demonstrate the high-sensitivity detection of coherent acoustic phonons with dephasing times in the range of the 100 ps time window.

OCIS codes: (320.7150) Ultrafast spectroscopy; (300.6500) Spectroscopy, time-resolved. (140.3425) Laser stabilization; (300.6320) Spectroscopy, high-resolution.

References and links

1. G. Sucha, "Rapid scanning time delays for ultrafast measurement systems," in *Ultrafast Lasers* (CRC, 2002).
2. P. A. Elzinga, F. E. Lytle, Y. Jian, G. B. King, and N. M. Laurendeau, "Pump/probe spectroscopy by asynchronous optical sampling," Appl. Spectrosc. **41**, 2–4 (1987).
3. Y. Takagi and S. Adachi, "Subpicosecond optical sampling spectrometer using asynchronous tunable mode-locked lasers," Rev. Sci. Instrum. **70**, 2218–2224 (1999).
4. G. Klatt, R. Gebs, C. Janke, T. Dekorsy, and A. Bartels, "Rapid-scanning terahertz precision spectrometer with more than 6 THz spectral coverage," Opt. Express **17**, 22847–22854 (2009).
5. T. Yasui, K. Kawamoto, Y.-D. Hsieh, Y. Sakaguchi, M. Jewariya, H. Inaba, K. Minoshima, F. Hindle, and T. Araki, "Enhancement of spectral resolution and accuracy in asynchronous-optical-sampling terahertz time-domain spectroscopy for low-pressure gas-phase analysis," Opt. Express **20**, 15071–15078 (2012).
6. A. Bartels, "Entwicklung von Femtosekundenlasern mit Repetitionsraten oberhalb 1 GHz und ihre Anwendungen," Ph.D. thesis, RWTH Aachen (2001).
7. A. Bartels, R. Cerna, C. Kistner, A. Thoma, F. Hudert, C. Janke, and T. Dekorsy, "Ultrafast time-domain spectroscopy based on high-speed asynchronous optical sampling," Rev. Sci. Instrum. **78**, 035107 (2007).
8. V. A. Stoica, Y.-M. Sheu, D. A. Reis, and R. Clarke, "Wideband detection of transient solid-state dynamics using ultrafast fiber lasers and asynchronous optical sampling," Opt. Express **16**, 2322–2335 (2008).
9. D. Stehr, C. M. Morris, C. Schmidt, and M. S. Sherwin, "High-performance fiber-laser-based terahertz spectrometer," Opt. Lett. **35**, 3799–3801 (2010).
10. J. Posthumus, "Terahertz with electronic delay - new sampling technique facilitates terahertz spectroscopy," Optik & Photonik **4**, 30 (2007).
11. Y. Kim and D.-S. Yee, "High-speed terahertz time-domain spectroscopy based on electronically controlled optical sampling," Opt. Lett. **35**, 3715 (2010).
12. S. Kray, F. Spöler, T. Hellerer, and H. Kurz, "Electronically controlled coherent linear optical sampling for optical coherence tomography," Opt. Express **18**, 9977 (2010).
13. T. Furuya, E. S. Estacio, K. Horita, C. T. Que, K. Yamamoto, F. Miyamaru, S. Nishizawa, and M. Tani, "Fast-scan terahertz time domain spectrometer based on laser repetition frequency modulation," Jpn. J. Appl. Phys. **25**, 022401 (2013).
14. T. Hochrein, R. Wilk, M. Mei, R. Holzwarth, N. Krumbholz, and M. Koch, "Optical sampling by laser cavity tuning," Opt. Express **18**, 1613–1617 (2010).

#280115 http://dx.doi.org/10.1364/OE.24.029930
Journal © 2016 Received 7 Nov 2016; revised 30 Nov 2016; accepted 1 Dec 2016; published 15 Dec 2016

Optics EXPRESS

15. L. Yang, J. Nie, and L. Duan, "Dynamic optical sampling by cavity tuning and its application in lidar," Opt. Express **21**, 3850–3860 (2013).
16. L. Knake, G. Schwaab, K. Kartaschew, and M. Havenith, "Solvation dynamics of trimethylamine n-oxide in aqueous solution probed by terahertz spectroscopy," J. Phys. Chem. B **119**, 13842–13851 (2015). PMID: 26214376.
17. B. F. Spencer, W. F. Smith, M. T. Hibberd, P. Dawson, M. Beck, A. Bartels, I. Guiney, C. J. Humphreys, and D. M. Graham, "Terahertz cyclotron resonance spectroscopy of an algan/gan heterostructure using a high-field pulsed magnet and an asynchronous optical sampling technique," Appl. Phys. Lett. **108**, 212101 (2016).
18. A. Bruchhausen, R. Gebs, F. Hudert, D. Issenmann, G. Klatt, A. Bartels, O. Schecker, R. Waitz, A. Erbe, E. Scheer, J.-R. Huntzinger, A. Mlayah, and T. Dekorsy, "Subharmonic resonant optical excitation of confined acoustic modes in a free-standing semiconductor membrane at GHz frequencies with a high-repetition-rate femtosecond laser," Phys. Rev. Lett. **106**, 077401 (2011).
19. Z. Feng, D. Liu, Z. Zuo, Q. Yu, R. Wang, and X. Xu, "Resonant actuation of microcantilever by pulse wave of one-nth the resonant frequency," Appl. Phys. Lett. **101**, 061901 (2012).
20. R. Gebs, G. Klatt, C. Janke, T. Dekorsy, and A. Bartels, "High-speed asynchronous optical sampling with sub-50fs time resolution," Opt. Express **18**, 5974–5983 (2010).
21. A. Bartels, D. Heinecke, and S. A. Diddams, "Passively mode-locked 10 GHz femtosecond Ti:sapphire laser," Opt. Lett. **33**, 1905–1907 (2008).
22. A. Bartels, D. Heinecke, and S. A. Diddams, "10-GHz self-referenced optical frequency comb," Science **326**, 681 (2009).
23. L. Rothman, I. Gordon, Y. Babikov, A. Barbe, D. C. Benner, P. Bernath, M. Birk, L. Bizzocchi, V. Boudon, L. Brown, A. Campargue, K. Chance, E. Cohen, L. Coudert, V. Devi, B. Drouin, A. Fayt, J.-M. Flaud, R. Gamache, J. Harrison, J.-M. Hartmann, C. Hill, J. Hodges, D. Jacquemart, A. Jolly, J. Lamouroux, R. L. Roy, G. Li, D. Long, O. Lyulin, C. Mackie, S. Massie, S. Mikhailenko, H. Müller, O. Naumenko, A. Nikitin, J. Orphal, V. Perevalov, A. Perrin, E. Polovtseva, C. Richard, M. Smith, E. Starikova, K. Sung, S. Tashkun, J. Tennyson, G. Toon, V. Tyuterev, and G. Wagner, "The {HITRAN2012} molecular spectroscopic database," J. Quant. Spectrosc. Radiat. Transfer **130**, 4 – 50 (2013). {HITRAN2012} special issue.
24. G. Klatt, R. Gebs, H. Schäfer, M. Nagel, C. Janke, A. Bartels, and T. Dekorsy, "High-resolution terahertz spectrometer," IEEE J. Select. Topics Quantum Electron. **17**, 159–168 (2011).
25. B. Born and M. Havenith, "Terahertz dance of proteins and sugars with water," J. Infrared Millim. Terahertz Waves **30**, 1245–1254 (2009).
26. A. Dreyhaupt, S. Winnerl, T. Dekorsy, and M. Helm, "High-intensity terahertz radiation from a microstructured large-area photoconductor," Appl. Phys. Lett. **86**, 121114 (2005).
27. S. Casalbuoni, H. Schlarb, B. Schmidt, P. Schmüser, B. Steffen, and A. Winter, "Numerical studies on the electro-optic detection of femtosecond electron bunches," Phys. Rev. ST Accel. Beams **11**, 072802 (2008).
28. M. van Exter, C. Fattinger, and D. Grischkowsky, "Terahertz time-domain spectroscopy of water vapor," Opt. Lett. **14**, 1128–1130 (1989).
29. H. Pickett, R. Poynter, E. Cohen, M. Delitsky, J. Pearson, and H. Müller, "Submillimeter, millimeter, and microwave spectral line catalog," J. Quant. Spectrosc. Radiat. Transfer **60**, 883–890 (1998).
30. P. Friberg, A. Hjalmarson, S. Madden, and W. M. Irvine, "Methanol in dark clouds," Astron. Astrophys. **195**, 281–289 (1988).
31. D. Riemer, W. Pos, P. Milne, C. Farmer, R. Zika, E. Apel, K. Olszyna, T. Kliendienst, W. Lonneman, S. Bertman, P. Shepson, and T. Starn, "Observations of nonmethane hydrocarbons and oxygenated volatile organic compounds at a rural site in the southeastern united states," J. Geophys. Res. Atmos. **103**, 28111–28128 (1998).
32. T. Yasui, Y. Iyonaga, Y.-D. Hsieh, Y. Sakaguchi, F. Hindle, S. Yokoyama, T. Araki, and M. Hashimoto, "Super-resolution discrete fourier transform spectroscopy beyond time-window size limitation using precisely periodic pulsed radiation," Optica **2**, 460–467 (2015).
33. A. Bartels, T. Dekorsy, H. Kurz, and K. Köhler, "Coherent zone-folded longitudinal acoustic phonons in semiconductor superlattices: Excitation and detection," Phys. Rev. Lett. **82**, 1044–1047 (1999).
34. K. Mizoguchi, M. Hase, S. Nakashima, and M. Nakayama, "Observation of coherent folded acoustic phonons propagating in a GaAs/AlAs superlattice by two-color pump-probe spectroscopy," Phys. Rev. B **60**, 8262–8266 (1999).
35. N. D. Lanzillotti-Kimura, A. Fainstein, A. Huynh, B. Perrin, B. Jusserand, A. Miard, and A. Lemaître, "Coherent generation of acoustic phonons in an optical microcavity," Phys. Rev. Lett. **99**, 217405 (2007).
36. C. Colvard, R. Merlin, M. V. Klein, and A. C. Gossard, "Observation of folded acoustic phonons in a semiconductor superlattice," Phys. Rev. Lett. **45**, 298–301 (1980).

1. Introduction

Scanning dual laser systems [1] have proven as valuable tools for time-resolved sampling in applications like optical pump-probe [2, 3] or THz time domain spectroscopy [4, 5]. In these systems, the time delay between two pulse trains emitted by mode-locked laser oscillators is generated by modulating the resonator length instead of using a mechanical optical delay line.

Optics EXPRESS

This allows to achieve very high scan rates in the kHz range of the time delay window. Using two lasers with slightly detuned repetition rates gives rise to a time delay increment between successive pulse pairs. The probe pulse samples the time delay window until the pulses coincide again after the scan time $T_{\mathrm{scan}} = 1/\Delta f$, defined by the repetition rate offset frequency Δf. This technique is referred to as asynchronous optical sampling (ASOPS) [2, 6] and can be seen as the optical counterpart to the equivalent time sampling method. The time delay increment is given by $\Delta\tau = (\Delta f)/(f_{\mathrm{R}} \cdot (f_{\mathrm{R}} + \Delta f)) \approx (\Delta f)/(f_{\mathrm{R}}^2)$, [7]. Increasing the laser repetition rate f_{R} allows for larger repetition rate offset frequencies Δf, reducing the measurement time T_{scan}, but keeping the time delay increment constant. Important to note is the quadratic dependency of $\Delta\tau$ on the repetition rate. Therefore, increasing the repetition rate by a factor of 10 allows to increase the repetition rate offset by a factor of 100 and keeping $\Delta\tau$ constant. The time delay window is given by $T_W = \frac{1}{f_{\mathrm{R}}}$. Thus, a high repetition rate results in a shorter time delay window. Fig. 1 shows the scan rate versus the length of the time delay window for different systems using ASOPS [3, 7–9] and ASOPS-related configurations [10–15]. For applications like terahertz time-domain spectroscopy (THz-TDS), a time window of only a few tens of ps is often sufficient. When using a low repetition rate ASOPS system, for example, 80 MHz, most of the time window of 12.5 ns does not contain useful information of interest. Electronically controlled optical sampling [10–12] circumvents this by scanning only a part of the time delay window, but special care must be taken for synchronizing of the scanning time-delay generation and data acquisition. In this work an ASOPS system based on femtosecond lasers with repetition rates of 10 GHz is implemented, compare Fig. 1. The high repetition rates allow for scan frequencies of up to 200 kHz of the 100 ps long time window corresponding to a scan speed of 20 $\frac{\mathrm{ps}}{\mu\mathrm{s}}$, however for practical reasons a scan speed of 100 kHz is typically used. Figure 1 also shows the relationship between offset frequency and time-delay resolution for different repetition rates of ASOPS systems. Using high scan speeds of dual-scanning laser systems can allow to reduce the total measurement time. Beside the general benefit of a short data acquisition time this can allow for measurements on the sub-second timescale as for example monitoring of hydration dynamics [16] or spectroscopy

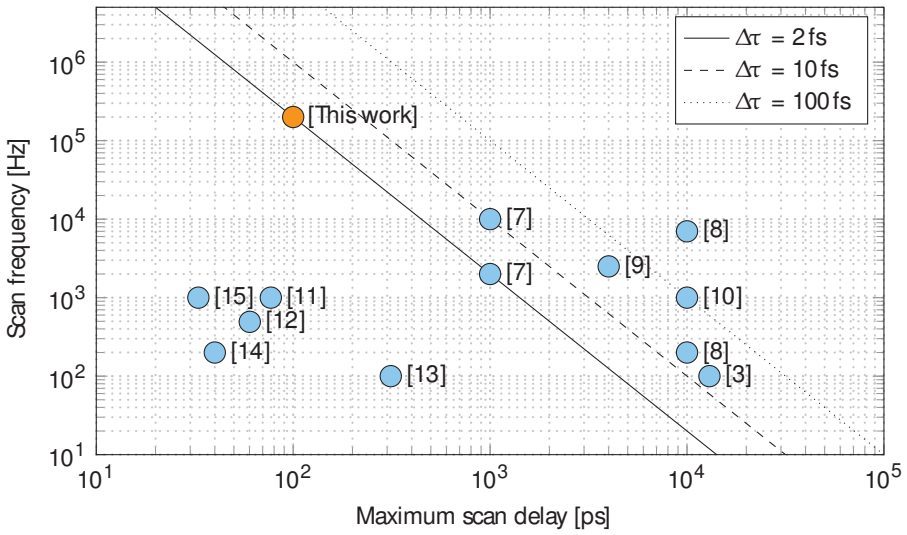

Fig. 1. Scan delay versus scan frequency for implementations of ASOPS and ASOPS-related dual scanning laser spectroscopy systems. The lines indicate offset or scan frequency versus maximum scan delay (i.e. the inverse repetition rate) for different time-delay resolutions in ASOPS implementations.

Optics EXPRESS

on magnetic fields [17]. Another application which benefits from the high repetition rate is the resonant excitation of nanostructures for determining lifetimes of acoustic modes with ultra-high Q factors. If the phonon life time exceeds the time-delay window, it is difficult to extract correct phonon life times. However, driving the mode resonantly and increasing the amount of energy stored in the oscillation allows to extract the quality factor by measuring the enhancement factor as a function of driving frequency. This has been demonstrated driving a silicon membrane on the 19^{th} subharmonic [18] and for electrical driving on the 7^{th} subharmonic of a microcantilever system [19]. By decreasing the sub-harmonic order by increasing the repetition rate enhances this effect greatly since less energy can be dissipated before the next excitation pulse arrives.

2. 10 GHz Asynchronous optical sampling setup

Establishing an ASOPS measurement scheme requires careful synchronization of the repetition rate offset between the deployed laser oscillators. The setup used for synchronizing two Ti:sapphire oscillators with 10 GHz is shown in Fig. 2. The implementation of the repetition rate offset stabilization is based on an earlier design for an ASOPS system using 1 GHz repetition rate oscillators [20] however several changes have become necessary at 10 GHz repetition rate due to the limited availability and cost of equivalent components in the high-frequency RF regime. The core part of the whole system are two Ti:sapphire femtosecond lasers with 10 GHz pulse repetition rate [21, 22] colocated in a common unibody aluminum housing. Both lasers operate at a central wavelength of about 780 nm and deliver about 600 mW of output power. The Fourier-limited pulse duration is $\approx$ 60 fs. Each laser is equipped with a set of two piezo-electric transducers (PZTs) with $\approx$ 1 kHz and 10 kHz bandwidth for active cavity length stabilization. The output-coupling mirror is mounted on a piezo-actuated stage for repetition rate tuning. The tuning range while the laser is mode-locked is up to ±30 MHz.

The setup allows for an active electronic stabilization of the repetition rate offset and the absolute repetition rate of the two oscillators. For this purpose a small portion of the output power is split of using the beam splitters BS1/BS3 and BS2/BS4 and focused onto two GaAs photodetectors with a 3 dB bandwidth of more than 12.5 GHz. Another part of the light from each laser is used for the generation of an optical trigger signal. The band-pass filters BP1 and BP2 following the photodiodes PD1 and PD2 isolate the fundamental repetition rate signals at f_R and $f_R + \Delta f$. These signals are used to generate coherent error signals corresponding to any deviations from the desired repetition rate $f_{R,set} = 10 \cdot f_{synth}$ and Δf_{set} for the absolute and offset repetition rate stabilization respectively. The oscillators running at repetition rates f_R and $f_R + \Delta f$ will serve as pump and probe laser for pump-probe experiments and are referred to as "master" and "slave" laser in the following description.

In the master signal path the signal is split again and fed into a frequency divider and a subsequent band-pass BP3 reducing the frequency to one tenth of the master repetition rate. This step is necessary because the maximum input frequency of the following direct-digital-synthesis (DDS) devices is limited to $\approx$ 1 GHz. DDS1 is configured to output a fixed output frequency of $f_{DDS} = 400$ MHz whereas DDS2 has an output frequency of $f_{DDS} - \Delta f_{set}$. The signals of DDS1 and DDS2 are then mixed at M2 and M3 with the master repetition rate signal and the slave repetition rate signal. The band-pass filters BP4 and BP5 filter the upper sideband of both mixers which results in signals with the sum of the input frequencies. A final mixing step at mixer M4 substracts these two signals removing the influence of f_R and f_{DDS} and provides the error signal which is proportional to $\Delta f - \Delta f_{set}$. The error signal is fed into a feedback unit to complete the phase-locked loop keeping the repetition rate offset between the oscillators stabilized. This unit consists of a PI-filter, a frequency diplexer to distribute the servo signal to the the fast and slow PZTs inside the laser cavity and a high-voltage amplifier. A second feedback unit is available to stabilize the absolute repetition rate of the master oscillator. For the error signal generation

Optics EXPRESS

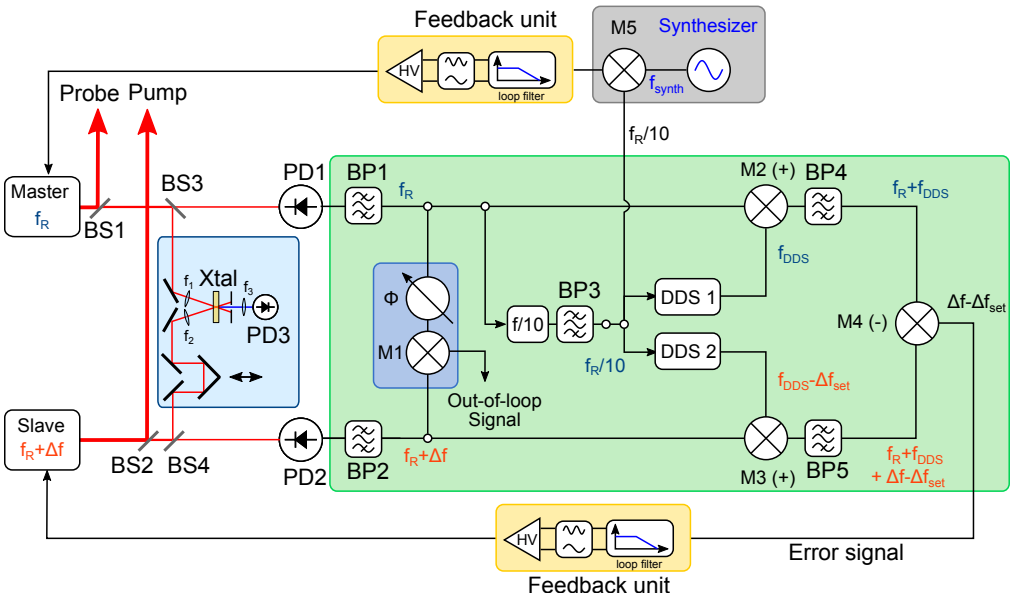

Fig. 2. Stabilization scheme of the 10 GHz ASOPS system. The optical path is depicted in solid red lines and all electronic connections are indicated with solid black lines. The blue box contains the optical trigger based on non-colinear sum frequency generation. The green box covers the offset error signal generation whereas the upper gray box shows the generation of a second error signal for absolute repetition rate stabilization of the master oscillator. The blue and orange color highlights the signals paths of the master and slave repetition rate signals respectively. **BS1-4**: optical beam-splitters. **f1-2**: $f = 100$ mm lenses. **f3**: $f = 50$ mm lens. **Xtal:** 2 mm long bismuth triborate crystal. **PD1-2**: GaAs photodiodes with > 12.5 GHz bandwidth. **PD3**: Amplified Si-photodiode with 125 MHz bandwidth. **BP1-4**: electronic band-pass filters. Φ variable electronic phase shifter. **DDS1-2**: 14-bit direct digital synthesizers. **M1-M5**: electronic mixers. Each feedback unit consists of a PI-filter, a frequency diplexer and a high voltage (HV) amplifier.

the divided signal at $f_R/10$ is mixed at M5 with a local oscillator signal at f_{synth} provided by a frequency synthesizer.

The light reflected at the beam splitters BS1 and BS2 is used for ultrafast time-domain spectroscopy in particularly laser induced transient transmission and reflectivity changes as well as terahertz generation and electro-optical sampling. In all conducted experiments the probe beam is detected by a photoreceiver with 125 MHz AC bandwidth and 50 kHz DC bandwidth. Measuring the ratio of AC and DC signal can be used to obtain the differential transmission $\Delta T/T$ or reflectivity $\Delta R/R$ if necessary. The analog signals are digitized using a 1 GS/s A/D converter with 12-bit nominal resolution. As ASOPS is usually combined with multi-transient averaging as noise reduction technique, a precise temporal stacking of the acquired pump-probe transients is paramount. For this purpose an optical trigger signal is generated by means of a cross-correlation between the master and slave laser at the photoreceiver PD3. A minimum of 50 mW per laser is split of at the beam splitters BS2 and BS4. One beam traverses a variable delay line to delay the pulses with respect to the other laser. This allows to shift the measured pump-probe signal within the time-window by tuning the relative temporal delay between the trigger and measurement signal. The beams are then non-colinearly focused onto a 2 mm long bismuth triborate (BiBO) crystal which is cut for type-I critical phase matching. In the crystal the sum frequency between both lasers is generated. The non-collinear geometry offers the advantage of having a background

Optics EXPRESS

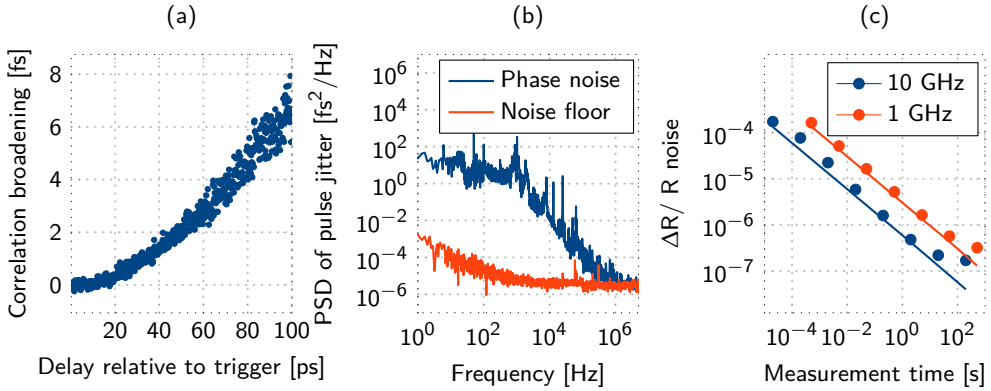

Fig. 3. (a) Correlation broadening due to timing jitter in the ASOPS system relative to the trigger event. (b) Power spectral density of the relative timing jitter between the two oscillators. (c) Noise floor comparison of a 1 GHz and 10 GHz pump-probe spectroscopy setup versus measurement time. The solid lines indicate the shot noise while the measured noise is indicated by dots.

free signal where the fundamental frequency and residual second harmonic generation can be blocked by an aperture behind the crystal. The single-shot signal-to-noise ratio of the trigger signal is 25 dB when using 50 mW of power per laser which is sufficient for reliable triggering and averaging of the acquired single-shot transients.

3. Characterization of the system performance

An important difference of ASOPS based time-domain spectroscopy compared to single oscillator based systems is the way the time-axis is calibrated. Converting the sample number given by the A/D converter into a time delay $\Delta\tau$ assumes a constant repetition rate offset Δf. Despite the PLL enforced stabilization of the repetition rate offset a residual jitter of Δf due to the finite loop bandwidth remains. The residual jitter is caused by the relative phase noise between both oscillators and should be smaller than the laser pulse length to avoid distortions of the measured transients. This effect is studied in two different ways. A sum-frequency generation setup with the same geometry as the optical trigger shown in Fig. 2 is used to measure the effect of timing jitter on the cross-correlation signal between both oscillators. Both oscillators are locked to $\Delta f = 100$ kHz using a master repetition rate of $f_R = 9.980\,91$ GHz as described in the previous section. The only difference between the two sum-frequency generations is the lack of the variable delay line and the use of a 250 µm long BiBO crystal in the characterization setup.

The measured cross-correlation signal is shifted through the time window of 100 ps by shifting the variable delay line in the optical trigger with a 25 µm increment. The width of the correlation is determined and the change of the correlation width is shown in Fig. 3(a). The correlation broadens from 160 fs by an average of about 7 fs at the end of the time window. This value is well below the Fourier-limited pulse duration of 60 fs and will not lead to significant signal distortions. At an offset frequency of 100 kHz corresponding to 10 µs single-shot acquisition time the oscillators are effectively free running as the bandwidth of the intracavity-PZTs is at least one order of magnitude smaller.

To further study the timing jitter the relative phase noise between both oscillators has been measured and is shown in Fig. 3(b). A part of the signal from both photodiodes (see Fig. 2) PD1 and PD2 is split to generate an out-of-loop signal for characterizing the offset synchronization of the lasers. A variable phase shifter is used in order to use the following double balanced

Optics EXPRESS

mixer M1 in the linear regime where the output is proportional to $\sin(\Delta\phi(t)) \approx \Delta\phi(t)$ for small phase fluctuations. If the offset Δf between both lasers is synchronized to zero frequency the out-of-loop signal can be used to measure the relative phase noise between both oscillators. The out-of-loop signal is analyzed by two signal analyzers with a bandwidth from DC to 102.4 kHz and from 100 kHz to 10 MHz respectively. Both signals have been stitched together in Fig. 3(b). The phase noise spectrum exhibits a flat baseline up to 1 kHz before starting to fall of with a $1/f$-behavior. A clear influence of AM to PM-conversion from pump laser amplitude noise is visible as distinct peaks in the noise spectrum. A lower correlation broadening could be achieved by either using faster PZTs or by reducing the relative phase noise between both lasers. The most relevant part of the spectrum lies above the repetition rate offset as this part directly affects the time calibration during the acquisition of a single transient. Therefore using high repetition rate offsets is advantageous due to the smaller phase noise at high frequencies.

Using high repetition rate offsets also improves the measurement speed. As the time increment scales inversely quadratic with the repetition rate f_R up to 100 times faster measurement speeds compared to 1 GHz systems while maintaining the same time increment can be achieved. However the requirements concerning A/D converters and detection bandwidth increases as well. Figure 3(c) shows the measured differential reflectivity noise floor versus measurement time of a 10 GHz and a 1 GHz system in comparison. For both measurements 5 mW of optical power have been measured by a 125 MHz bandwidth Si-photoreceiver leading to identical shot-noise for both systems. Both systems operate close to the shot-noise limit. Residual low-frequency amplitude noise of the oscillators limits reaching the shot-noise limit. For long measurement times the noise reduction no longer follows a $\propto 1/\sqrt{N}$ behaviour where N is the number of averaged transients. The reason for this deviation is the technical noise of the A/D converter which dominates the noise floor for long measurement times. For the 10 GHz system a low noise floor can be reached within a shorter measurement time. This is can be understood by the fact that the same shot noise voltage is sampled and averaged using 10 µs long segments for the 10 GHz ASOPS system and 1 ms long segments for the 1 GHz ASOPS system. However the present system is limited by the trigger dead time of the used A/D converter which is 4 µs. Due to the trigger dead time only every second transient is acquired increasing the theoretical possible measurement time by a factor of two.

4. Terahertz time-domain spectroscopy

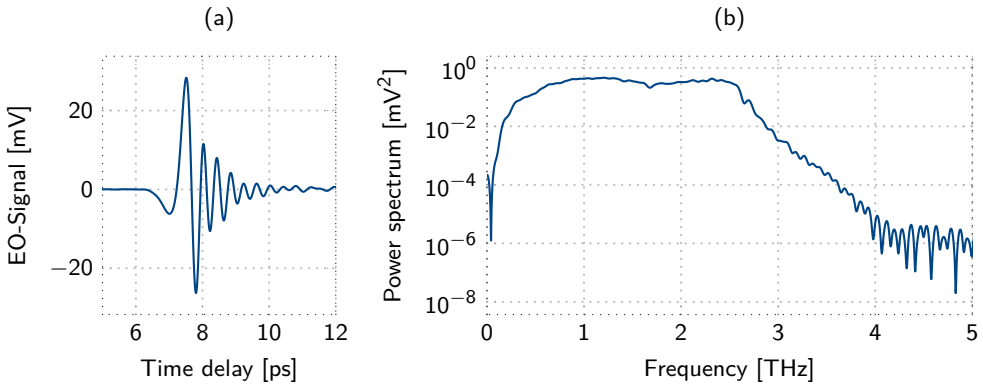

Fig. 4. (a) Single THz pulse in the time domain. (b) Fourier transform power spectrum of a single THz pulse.

Optics EXPRESS

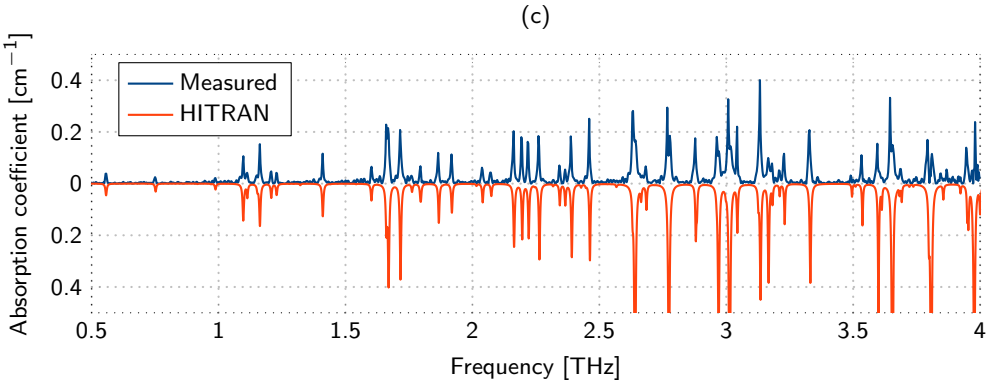

Fig. 5. Measured absorption spectrum of H_2O vapor in a 20 cm long absorption path. As a comparison a calculated spectrum using the HITRAN spectroscopy database [23] is shown. The measurement consists of 10.24 million averaged time-domain traces which have been acquired in 204.8 seconds.

Performing terahertz time-domain spectroscopy at high repetition rates is an interesting application [4, 24] as the relevant time window usually only covers a few tenth of picoseconds and a 10 GHz frequency resolution is still sufficient for many samples. The high scan rate is also advantageous for experiments on two time scales using the setup for kinetic terahertz absorption spectroscopy [25].

To test the 10 GHz ASOPS system a simple terahertz time-domain spectrometer has been set up. 300 mW optical power of the pump beam was focused down to a 60 µm spot size on a large area LT GaAs photoconductive emitter [26]. The generated terahertz radiation is collected and focused on a 500 µm thick zinc-telluride (ZnTe) crystal with a pair of 1″ off-axis parabolic mirrors with a f-number of 1. The probe beam is overlapped through a hole in the focusing mirror on the ZnTe crystal. The used probe power is 300 mW. A quarter wave-plate and a polarizing beam splitter cube conclude the unbalanced electro-optic sampling setup before focusing 5 mW of the transmitted probe light onto the detector. The total length of the terahertz beam path is 20 cm. For all THz measurements the master repetition rate was $f_R = 10.0$ GHz and the repetition rate offset was locked to $\Delta f = 100$ kHz. Figure 4(a) shows a single acquired terahertz pulse. The setup has been purged with dry synthetic air to reduce water absorption. The power spectrum of this terahertz pulse is shown in Fig. 4(b). The measurement time was 204.8 seconds and the achieved dynamic range is 67 dB. The spectrum shows a terahertz spectrum spanning from almost DC up to 4 THz. The steep decline of the terahertz power starting at 2.5 THz is due to the nonlinear response function of the used ZnTe-crystal as the group and phase velocity matching condition is no longer fulfilled [27].

Verification of the terahertz spectrometer is done by measuring the absorption spectrum of water vapor [28]. A terahertz spectrum was acquired at room temperature (296 K) with 42 % relative humidity at 965 hPa ambient pressure. The errors of these parameters are ±1 K, ±2 % and ±5 hPa respectively. The absorption coefficient α is retrieved from the complex Fourier spectra of the sample and reference measurement. The measured absorption coefficient is plotted in Fig. 5 in the upper part of the axis of the ordinate and a HITRAN spectrum on the lower part. The HITRAN spectrum has been calculated using the equations given in [23] and the latest version of the database has been used. For the parameters given above the linewidth of the water absorption lines is on the order of 5 to 10 GHz and is therefore on the same order as the frequency resolution of the setup. A single absorption line is therefore sampled by only one line of the terahertz frequency comb generated by the photo-conductive emitter. Depending on the absolute

Optics EXPRESS

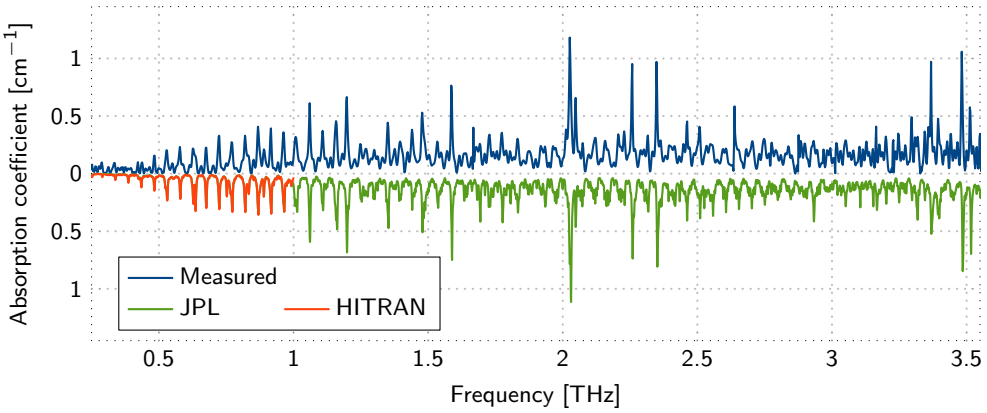

Fig. 6. Measured absorption spectrum of gaseous methanol (CH_3OH) in a 5 cm long gas cell at 133.5 hPa. A comparison with the HITRAN spectroscopy database [23] up to 1 THz is shown and with the JPL database [29] which provides data also for frequencies above 1 THz.

value of the frequency comb line frequency the absorption line is not sampled at the center of the line which leads to deviations in the measured absorption coefficient. At frequencies above 2.5 THz the dynamic range of the spectrometer starts to decrease which further limits the ability to resolve and quantifiy the absorption coefficient correctly. Despite these limitations almost all lines predicted by the HITRAN calculations are resolved by the THz-TDS setup.

Methanol (CH_3OH) in its gaseous state is of high importance for astronomic studies of the interstellar medium e.g. in dark clouds [30] and for atmospheric trace gas sensing [31]. A compact gas cell with 5 cm path length and wedged TPX windows is added to the setup in the collimated THz beam path between the off-axis parabolic mirrors. The cell is filled with 1 ml of liquid methanol and then pumped down to remove air and water vapor from the cell forming a closed system of liquid and gaseous methanol. The gaseous methanol has a vapor pressure of 133.5 hPa at 293.5 K. Figure 6 shows the measured absorption spectrum of gaseous methanol. The measured spectrum is compared to the HITRAN database and the molecular spectroscopy database of the Jet Propulsion Laboratory (JPL) [29] as the HITRAN database does not cover the entire measurement bandwidth. The JPL database lists no parameters for pressure and self broadening, therefore these parameters have been taken from the HITRAN database as they are listed as constant for all lines. For the calculation $\sim$ 11000 lines with a line strength of more than 3.3×10^{-23} cm^{-1}/(molecule /cm^2) have been included. The resulting spectrum is in good agreement with the measured spectrum and the calculated HITRAN spectrum. Due to the pressure broadening of the absorption lines a continuous absorption background is present with some strong absorption lines sticking out of the absorption background. Resolving absorption features at low methanol pressures could be achieved by sweeping the repetition rate of the pump laser and tuning the generated THz frequency comb to the gas absorption lines of interest [32].

5. Pump-probe spectroscopy in semiconductor superlattices

Coherent acoustic phonons in GaAs/AlAs semiconductor superlattices have been studied extensively in order to investigate picosecond ultrasonics by means of pump-probe spectroscopy [33, 34]. The dispersion of acoustic phonons in a superlattice exhibits a back-folding to a mini-Brillouin zone which is formed due to the periodicity of the structure. Upon laser excitation this leads to the formation of high-frequency back-folded longitudinal acoustic phonons. In [33] the excitation and detection mechanisms have been identified as impulse stimulated Raman

Optics EXPRESS

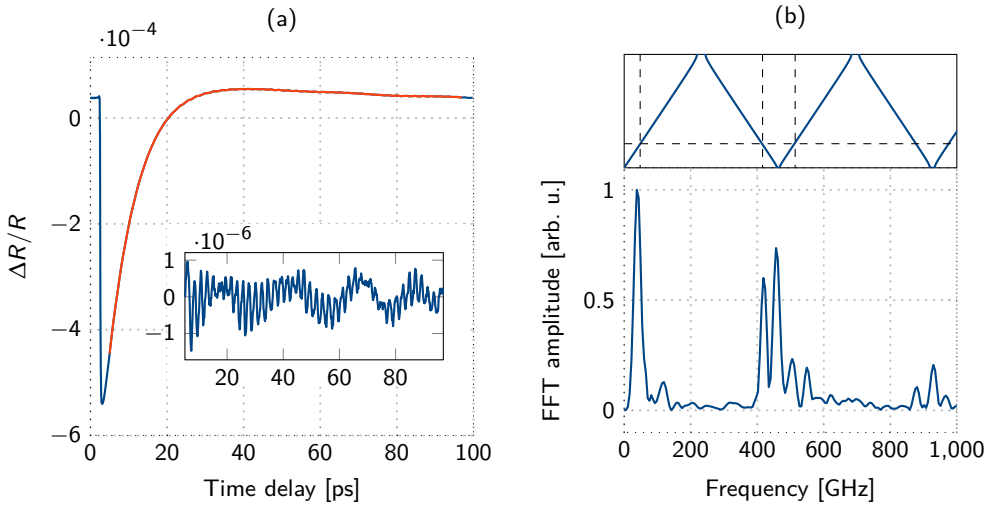

Fig. 7. (a) Measured pump-probe transient in the GaAs/AlAs superlattice. Highlighted in red is the part of the transient used for evaluation. The inset shows the extracted acoustic phonons after background extraction. (b) Interpolated FFT spectrum of the data shown in the inset of (a). On top of the plot the calculated dispersion relation is plotted. Dashed vertical lines indicate the predicted acoustic phonon frequencies.

scattering and the acoustic deformation potential respectively. The generation and detection efficiency scales with the pulse energy of the pump and probe laser respectively [35]. Despite this strongly reduced efficiency, the 10 GHz ASOPS system is a very interesting system for pump-probe experiments for acoustic phonon cavities based on GaAs/AlAs superlattices [35] as the high pulse repetition rate could allow for sub-resonant or even resonant driving of the acoustic cavity mode [18].

In this experiment a GaAs/AlAs superlattice has been studied to show the potential of the 10 GHz ASOPS system to detect and resolve very small reflectivity changes. The superlattice structure is formed by 40 periods grown on a (001) orientied GaAs substrate. Each period consists of 19 monolayers of the two constituents. 100 mW of the pump laser are focused through a 40 mm lens under an angle onto the sample surface. For probing the induced dynamics 10 mW of the probe laser are focused using a 30 mm lens and the back-reflected light is collected through the same lens, split-off and focused onto a 125 MHz photoreceiver. The used repetition rate was $f_R = 10.011\,25$ GHz and the repetition rate offset was $\Delta f = 100$ kHz. The measured transient after 10.24 million averages is shown in 7(a). The total measurement time was again 204.8 seconds. The red solid part of the curve marks the evaluated subset of the transient from 5 ps to 97 ps. The inset shows the extracted oscillations by removing the background carrier dynamics. The signal shows a decaying oscillation with a strong beat modulation. To identify the individual contributions the Fourier spectrum is calculated and plotted in Fig. 7(b). The upper part of the graph shows the calculated dispersion relation using the Rytov model. Material density and sound velocity parameters have been taken from [36] and the individual layer thickness have been fitted to 5.59 nm for the GaAs layer and 5.46 nm for the AlAs layer to match the experimental data. The spectrum shows three distinct contributions to the oscillatory behaviour. The two tripplets at 460 GHz and 920 GHz can be identified as the first- and second-branch zone-center mode and the back-scattered $q = 2 \cdot k_{\text{laser}}$ Raman modes. The strong low-frequency modulation can be identified as Brillouin oscillation at a frequency of 50 GHz.

Optics EXPRESS

6. Conclusion

We have presented a time-domain spectroscopy system based on two Ti:sapphire oscillators with 10 GHz repetition rate. To our knowledge this is the highest pulse repetition rate ever used for pump-probe spectroscopy using Ti:sapphire lasers. At a repetition rate offset of 100 kHz and above this asynchronous optical sampling system reaches a pump-probe noise floor of 10^{-6} in less than one second and allows measuring close to the shot noise limit. The temporal resolution is 100 fs which is at the moment limited by chromatic dispersion in the setup as no pulse compression is applied. A timing jitter induced signal distortion of less than 10 fs is achieved. To demonstrate the capabilities of the system broadband terahertz absorption spectra of water vapor and gaseous methanol have been measured and compared to spectroscopic databases. Furthermore the ability to detect 10^{-7} reflectivity changes was validated by measuring coherent zone-folded acoustic phonons in a semiconductor superlattice in accordance to earlier experiments with lower repetition rate systems. This new 10 GHz asynchronous optical sampling system enables advanced experiments like resonant driving of acousting excitations, line-by-line pulse shaping, dual-comb sampling and kinetic terahertz absorption spectroscopy.

Funding

German Research Foundation (DFG) Collaborative Research Center 767; German Research Foundation (DFG) Center for Applied Photonics, funded by the German Excellence Initiative.

Acknowledgments

Oliver Kliebisch thanks the Carl-Zeiss foundation (Stuttgart, Germany) for financial support.